International Journal of Fluid Mechanics & Thermal Sciences
2026, Vol. 12, No. 2, pp. 32–50
https://doi.org/10.11648/j.ijfmts.20261202.12

Research Article

Flow and Heat Transfer Through Vertical Channel with Radiation and Chemical Reaction in the Presence of Magnetic Field

Sanhita Paul[1], **Mrinmoy Guria**[2, *], **Sovan Lal Maji**[2]

[1]Department of Physics, Ghatal Rabindra Satabarsiki Mahavidyalaya, Ghatal, India
[2]Department of Mathematics, Ghatal Rabindra Satabarsiki Mahavidyalaya, Ghatal, India

Abstract

A study has been carried out to investigate the three–dimensional free convective heat and mass transfer flow of a viscous incompressible fluid within a vertical channel. The analysis considers the combined effects of thermal radiation and a chemical reaction, which are important in many engineering and industrial processes such as energy systems, cooling devices, and chemical processing units. The presence of a magnetic field is also taken into account because it significantly influences the motion of electrically conducting fluids. The governing equations representing the conservation of momentum, energy, and concentration are formulated under appropriate physical assumptions. These equations are nonlinear and coupled in nature; therefore, they are first transformed into non–dimensional form using suitable similarity parameters. An approximate analytical solution of the resulting equations is then obtained by applying a perturbation technique. This method enables the determination of velocity, temperature, and concentration distributions inside the vertical channel and helps in analysing the influence of different physical parameters on the flow characteristics. The results reveal several important features of the flow. In the case of a cooling plate, the primary velocity component decreases with an increase in the magnetic parameter, chemical reaction parameter, Prandtl number, and Schmidt number. The magnetic field introduces a resistive force, which tends to slow down the fluid motion. Similarly, larger values of the Prandtl and Schmidt numbers reduce thermal and mass diffusivity, leading to a reduction in fluid velocity. On the other hand, the primary velocity increases with increasing values of the thermal Grashof number and mass Grashof number, since these parameters represent buoyancy forces that enhance the fluid motion within the channel. It is also observed that the temperature distribution decreases with an increase in the Reynolds number, Prandtl number, and radiation parameter. Furthermore, the concentration field decreases when the Schmidt number, Reynolds number, or chemical reaction parameter increases, indicating a reduction in species diffusion within the fluid flow.

Keywords

Three-dimensional, Injection, Periodic Suction, Mass Transfer

*Correspondence: Mrinmoy Guria (mrinmoy9832@yahoo.com)

Received: 17 February 2026; **Accepted:** 23 March 2026; **Published:** 18 June 2026

1. Introduction

Natural convection accompanied by heat and mass transfer has been the subject of extensive investigation because of its important role in many scientific and engineering processes. Such flows arise due to density variations caused by temperature and concentration differences, leading to buoyancy-induced motion. These effects are commonly observed in atmospheric circulation, ocean currents, and even in geophysical systems within the Earth's interior. In a related study, Guria and Jana [1] analyzed three-dimensional flow in a vertical channel under the influence of periodic suction. However, their work did not incorporate thermal radiation, which becomes a key factor in several practical situations, particularly those involving very high temperatures. For instance, radiation plays a vital role in aerospace engineering problems such as the thermal analysis of re-entering space vehicles. High-temperature environments frequently encountered in advanced engineering systems—such as nuclear reactors, gas turbines, and propulsion units used in aircraft, missiles, satellites, and space crafts—intensify radiative heat transfer effects. In such conditions, neglecting radiation can lead to inaccurate predictions. Even in common domestic and industrial settings, natural convection is significant, such as in the warming of rooms by radiators and in heat dissipation from hot pipes, furnaces, and other equipment exposed to relatively cooler surroundings.

The influence of thermal radiation on fluid flow along a vertical plate has attracted considerable attention from researchers. Takhar et al. [2] analyzed the role of radiation in modifying the characteristics of flow past a vertical plate. Later, Guria et al. [3] examined the effect of radiative heat transfer on three-dimensional flow within a vertical channel subjected to periodic suction. Guria et al. [4] further extended their work to steady three-dimensional flow past a vertical porous plate under the action of a magnetic field, highlighting the interaction between radiation and magnetohydrodynamic forces.

The impact of periodic suction on three-dimensional mixed convection flow with simultaneous mass transfer was investigated by Singh and Thakar [5]. In another study, Ahmed [6] discussed heat and mass transfer characteristics in steady three-dimensional flow of a viscous incompressible fluid over a moving vertical plate. Subsequently, Ahmed and Liu [7] analyzed similar transport phenomena for flow past a vertical porous plate with a constant free stream velocity.

Further contributions by Reddy and Reddy [8] addressed unsteady magnetohydrodynamic free convection flow over a vertical porous plate, incorporating the combined effects of radiation, mass transfer, and viscous dissipation. More recently, Guria [9] conducted detailed investigations on heat and mass transfer in three-dimensional flow past a vertical porous plate, emphasizing the role of radiation. Additional studies by Guria [10] explored radiative effects in vertical channel flows, including analyses within the slip flow regime. Additionally, Guria [11] explored heat and mass transfer through a vertical channel with radiation effects. Further research by Guria [12] focused on heat and mass transfer through a vertical channel in the slip flow regime, and Guria [13] extended this work to include radiation effects through porous medium. Moreover, Zigta and Koya [14] examined the coupled influence of magnetic fields, radiation, and chemical reactions on free convection flow. Zigta [15, 16] also independently reported on the combined impact of radiation and chemical reactions in magnetohydrodynamic flow configurations.

The analysis of heat and mass transfer processes involving chemical reactions plays a vital role in chemical processing and hydrometallurgical operations. Chemical reactions are generally categorized into two types: homogeneous and heterogeneous. Homogeneous reactions take place uniformly within a single phase, whereas heterogeneous reactions occur at the interface between different phases or within a limited region. When the reaction rate is directly proportional to the concentration of the reacting species, the process is referred to as a first-order reaction. Many reactions are accompanied by either heat generation (exothermic) or heat absorption (endothermic), which significantly influence transport processes. Such phenomena are particularly relevant in industries such as polymer manufacturing, glass and ceramic production, and food technology.

Reddy et al. [17] analyzed three-dimensional magnetohydrodynamic flow and heat transfer in a porous medium with periodically varying permeability in the presence of chemical reactions. Sharma and Mahanta [18] studied the influence of chemical reactions on three-dimensional MHD heat and mass transfer over a vertical plate. In another investigation, Niranjana et al. [19] discussed the effects of chemical reactions on three-dimensional flow within a porous medium. The present study focuses on examining the combined influence of thermal radiation and chemical reaction on three-dimensional free convective heat and mass transfer flow in a vertical channel. Our present study is a non-trivial extension of Sharma and Mahanta [18], incorporating (i) the effect of radiation and (ii) flow through a vertical channel.

2. Basic Equations

We examine a steady-state flow of a viscous and incompressible fluid confined between two vertical, parallel porous plates separated by a distance d. The coordinate system is defined such that the x^*-axis is aligned with the primary flow direction, the y^*-axis is oriented perpendicular to the plates across the channel width, and the z^*-axis is taken normal to the x^*y^*-plane (Figure 1).

The plate located at $y^* = 0$ is maintained at a higher constant temperature T_w, while the opposite plate at $y^* = d$ is kept at a lower temperature T_0, with $T_w > T_0$.

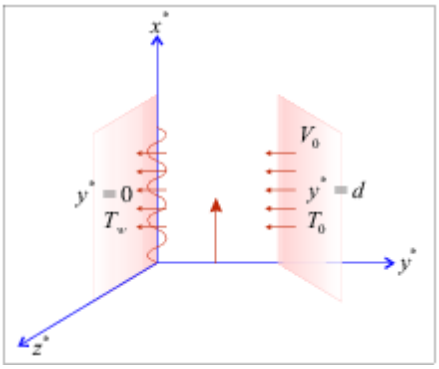

Figure 1. *Physical model and Co-ordinates system.*

The plate at $y^* = d$ experiences a constant injection velocity V_0, whereas the plate at $y^* = 0$ is exposed to a spatially varying suction given by

$$v^* = -V_0\left[1 + \varepsilon\cos\left(\frac{\pi z^*}{d}\right)\right] \quad (1)$$

where $\varepsilon(\varepsilon \ll 1)$ represents a small parameter indicating the magnitude of the periodic suction. Because the channel extends infinitely in the x^*-direction, all flow and thermal variables are independent of x^*. However, the presence of injection and periodic suction across the plates generates a cross-flow, making the motion inherently three-dimensional.

Let u^*, v^*, and w^*denote the velocity components along the x^*-, y^*-, and z^*-directions, respectively. The mathematical formulation of the problem is described by the following governing equations.

$$\frac{\partial v^\star}{\partial y^\star} + \frac{\partial w^\star}{\partial z^\star} = 0 \quad (2)$$

$$v^\star\frac{\partial u^\star}{\partial y^\star} + w^\star\frac{\partial u^\star}{\partial z^\star} = \nu\left(\frac{\partial^2 u^\star}{\partial y^{\star 2}} + \frac{\partial^2 u^\star}{\partial z^{\star 2}}\right) + g\beta + g\beta(C^* - C_0) - \frac{\sigma B_0^2}{\rho}u^* \quad (3)$$

$$v^\star\frac{\partial v^\star}{\partial y^\star} + w^\star\frac{\partial v^\star}{\partial z^\star} = -\frac{1}{\rho}\frac{\partial p^\star}{\partial y^\star} + \nu\left(\frac{\partial^2 v^\star}{\partial y^{\star 2}} + \frac{\partial^2 v^\star}{\partial z^{\star 2}}\right) \quad (4)$$

$$v^\star\frac{\partial w^\star}{\partial y^\star} + w^\star\frac{\partial w^\star}{\partial z^\star} = -\frac{1}{\rho}\frac{\partial p^\star}{\partial z^\star} + \nu\left(\frac{\partial^2 w^\star}{\partial y^{\star 2}} + \frac{\partial^2 w^\star}{\partial z^{\star 2}}\right) - \frac{\sigma B_0^2}{\rho}w^* \quad (5)$$

$$v^\star\frac{\partial T^*}{\partial y^\star} + w^\star\frac{\partial T^*}{\partial z^\star} = \frac{1}{\rho C_p}\left(\frac{\partial^2 T^*}{\partial y^{\star 2}} + \frac{\partial^2 T^*}{\partial z^{\star 2}}\right) - \frac{1}{\rho C_p}\frac{\partial q_r^*}{\partial y^*} \quad (6)$$

$$v^\star\frac{\partial C^*}{\partial y^\star} + w^\star\frac{\partial C^*}{\partial z^\star} = D\left(\frac{\partial^2 C^*}{\partial y^{\star 2}} + \frac{\partial^2 C^*}{\partial z^{\star 2}}\right) - \mathrm{K}^*(C^* - C_0) \quad (7)$$

Here, ν denotes the kinematic viscosity of the fluid, ρrepresents its density, and $p^*$is the pressure. The symbol g stands for gravitational acceleration, β is the coefficient of thermal expansion, and $C_p$indicates the specific heat at constant pressure. The parameter K^*corresponds to the rate constant associated with the chemical reaction.

The conservation of radiative heat transfer per unit volume, considering contributions over all wavelengths, can be expressed as

$$\nabla \cdot q_r^* = \int_0^\infty K_\lambda(T^*)[4e_{\lambda h}(T^*) - G_\lambda]d\lambda$$

where $e_{\lambda h}$ denotes the Planck distribution function. The incident radiation $G_\lambda$is defined by

$$G_\lambda = \frac{1}{\pi}\int_{\Omega=4\pi} e_\lambda(\Omega)\, d\Omega$$

with Ωrepresenting the solid angle and $\nabla \cdot q_r^*$indicating the divergence of the radiative heat flux.

For the case of an optically thin fluid interacting with an isothermal flat surface maintained at temperature T_0, and by applying Kirchhoff's law together with the above definition of radiative flux divergence, the incident radiation simplifies to

$$G_\lambda = 4e_{\lambda h}(T_0)$$

Under these assumptions, the radiative heat transfer expression can be further simplified accordingly.

$$\nabla . q_r^* = 4\int_0^\infty K_\lambda(T^*)(e_{\lambda h}(T^*) - e_{\lambda h}(T_0))d\lambda$$

Expanding $K_\lambda(T^*)$ and $e_{\lambda h}(T_0)$ in a Taylor series around T_0, for small $(T^* - T_0)$, we can rewrite the radiative flux divergence as

$$\nabla . q_r^* = 4(T^* - T_0)\int_0^\infty K_{\lambda_0}(\frac{\partial e_{\lambda h}}{\partial T})_0 d\lambda$$

where $K_{\lambda_0} = K_{\lambda(T_0)}$.

Hence an optical thin limit for a non-gray gas near equilibrium, the following relation holds

$$\nabla . q_r^* = 4(T^* - T_0)I$$

and hence

$$\frac{\partial q_r^*}{\partial y^*} = 4(T^* - T_0)I$$

where

$$I = \int_0^\infty K_{\lambda_0}(\frac{\partial e_{\lambda h}}{\partial T})_0 d\lambda$$

The boundary conditions of the problem are

$$u^\star = 0, v^\star = -V_0\left[1+\epsilon\cos\left(\frac{\pi}{d}z^\star\right)\right], w^\star = 0, T^* = T_w, C^* = C_w \text{ at } y^\star = 0$$

$$u^\star = 0, v^\star = -V_0, w^\star = 0, T^* = T_0, C^* = C_0, p^\star = p_\infty \text{ at } y^\star = d \tag{8}$$

Introducing the non dimensional variables

$$y = \frac{y^\star}{d}, z = \frac{z^\star}{d}, p = \frac{p^\star}{\rho V_0^2}, u = \frac{u^\star}{V_0}, v = \frac{v^\star}{V_0}, w = \frac{w^\star}{V_0}, \theta = \frac{(T^*-T_0)}{(T_w-T_0)} \tag{9}$$

equations (2)-(7) become

$$\frac{\partial v}{\partial y} + \frac{\partial w}{\partial z} = 0 \tag{10}$$

$$v\frac{\partial u}{\partial y} + w\frac{\partial u}{\partial z} = \frac{1}{Re}\left(\frac{\partial^2 u}{\partial y^2} + \frac{\partial^2 u}{\partial z^2}\right) + Gr\theta + GmC - Mu \tag{11}$$

$$v\frac{\partial v}{\partial y} + w\frac{\partial v}{\partial z} = -\frac{\partial p}{\partial y} + \frac{1}{Re}\left(\frac{\partial^2 v}{\partial y^2} + \frac{\partial^2 v}{\partial z^2}\right) \tag{12}$$

$$v\frac{\partial w}{\partial y} + w\frac{\partial w}{\partial z} = -\frac{\partial p}{\partial z} + \frac{1}{Re}\left(\frac{\partial^2 w}{\partial y^2} + \frac{\partial^2 w}{\partial z^2}\right) - Mw \tag{13}$$

$$v\frac{\partial \theta}{\partial y} + w\frac{\partial \theta}{\partial z} = \frac{1}{RePr}\left(\frac{\partial^2 \theta}{\partial y^2} + \frac{\partial^2 \theta}{\partial z^2}\right) - F\theta \tag{14}$$

$$v\frac{\partial C}{\partial y} + w\frac{\partial C}{\partial z} = \frac{1}{SRe}\left(\frac{\partial^2 C}{\partial y^2} + \frac{\partial^2 C}{\partial z^2}\right) - K_c C \tag{15}$$

where $Re = V_0 d/\nu$ is the Reynolds number, $Pr = \nu/\rho$ is the Prandtl number, $Gr = dg\beta(T_w - T_0)/V_0^2$ is the Grashof number, $Gm = dg\beta(C_w - C_0)/V_0^2$ is the mass Grashof number, $F = \frac{4Id}{\rho C_p V_0} is$ the radiation parameter, $S = \nu/D$ is the Schmidt number, $M = \frac{\sigma B_0^2}{\rho}\frac{d}{V_0}$ is the magnetic parameter and $K_c = \frac{K^* d}{V_0}$ is chemical reaction parameter. Using (9), the boundary conditions (8) become

$$u = 0, v = -\left[1+\epsilon\cos(\pi z)\right], w = 0, \theta = 1, C = 1, at\ y = 0$$

$$u = 0, v = -1, w = 0, \theta = 0, C = 0, p = \frac{p_\infty}{\rho V^2} \text{ at } y = 1 \tag{16}$$

3. Solution of the Problem

In order to solve the differential equations (10)-(15), we assume the solution of the following form

$$u(y,z) = u_0(y) + \epsilon u_1(y,z) + \epsilon^2 u_2(y,z) + \cdots$$

$$v(y,z) = v_0(y) + \epsilon v_1(y,z) + \epsilon^2 v_2(y,z) + \cdots$$

$$w(y,z) = w_0(y) + \epsilon w_1(y,z) + \epsilon^2 w_2(y,z) + \cdots \tag{17}$$

$$p(y,z) = p_0(y) + \epsilon p_1(y,z) + \epsilon^2 p_2(y,z) + \cdots$$

$$\theta(y,z) = \theta_0(y) + \epsilon\theta_1(y,z) + \epsilon^2\theta_2(y,z) + \cdots$$

$$C(y,z) = C_0(y) + \epsilon C_1(y,z) + \epsilon^2 C_2(y,z) + \cdots$$

On substituting (17) in equations (10)-(15) and equating the terms independent of ϵ, we get the following system of differential equations.

$$v_0' = 0 \tag{18}$$

$$u_0'' - Rev_0u_0' = -ReGr\theta_0 - ReGmC_0 + MReu_0 \tag{19}$$

$$\theta_0'' - RePrv_0\theta_0' - FRePr\theta_0 = 0 \tag{20}$$

$$C_0'' - SRev_0C_0' - SReK_cC_0 = 0 \tag{21}$$

where primes denotes differentiation with respect to y and the corresponding boundary conditions become

$$u_0 = 0, v_0 = -1, \theta_0 = 1, C_0 = 1 \text{ at } y = 0 \tag{22}$$

$$u_0 = 0, v_0 = -1, \theta_0 = 0, C_0 = 0 \text{ at } y = 1 \tag{23}$$

The solutions of the equations (18) to (21), subject to the

boundary conditions (22) are

$$v_0(y) = -1 \tag{24}$$

$$\theta_0(y) = \frac{1}{(e^{-\lambda_1} - e^{-\lambda_2})}\left[e^{-\lambda_1}e^{-\lambda_2 y} - e^{-\lambda_2}e^{-\lambda_1 y}\right] \tag{25}$$

$$C_0(y) = \frac{1}{(e^{-\lambda_4} - e^{-\lambda_3})}\left[e^{-\lambda_4}e^{-\lambda_3 y} - e^{-\lambda_3}e^{-\lambda_4 y}\right] \tag{26}$$

$$u_0(y) = \sum_{i=1}^{6} A_i e^{-\lambda_i y} \tag{27}$$

where

$$\lambda_{1,2} = \frac{1}{2}\left\{RePr \pm \sqrt{Re^2Pr^2 + 4FRePr}\right\}$$

$$\lambda_{3,4} = \frac{1}{2}\left\{SRe \pm \sqrt{S^2Re^2 + 4SReK_c}\right\}$$

$$\lambda_{5,6} = \frac{1}{2}\left\{Re \pm \sqrt{Re^2 + 4MRe}\right\}$$

$$K_1 = \frac{-ReGr}{(e^{-\lambda_2} - e^{-\lambda_1})}$$

$$K_2 = \frac{-ReGm}{(e^{-\lambda_4} - e^{-\lambda_3})}$$

$$A_1 = \frac{k_1 e^{-\lambda_2}}{\lambda_1^2 - Re\lambda_1 - MRe}$$

$$A_2 = \frac{-k_1 e^{-\lambda_1}}{\lambda_2^2 - Re\lambda_2 - MRe}$$

$$A_3 = \frac{k_2 e^{-\lambda_4}}{\lambda_3^2 - Re\lambda_3 - MRe}$$

$$A_4 = \frac{-k_2 e^{-\lambda_3}}{\lambda_4^2 - Re\lambda_4 - MRe}$$

$$A_5 = \frac{1}{(e^{-\lambda_6} - e^{-\lambda_5})}\sum_{i=1}^{4} A_i(e^{-\lambda_i} - e^{-\lambda_6}) \tag{28}$$

$$A_6 = \frac{-1}{(e^{-\lambda_6} - e^{-\lambda_5})}\sum_{i=1}^{4} A_i(e^{-\lambda_i} - e^{-\lambda_5})$$

On substituting (17) in equations (10)-(15) and equating the coefficient of ϵ, we get the following system of differential equations.

$$\frac{\partial v_1}{\partial y} + \frac{\partial w_1}{\partial z} = 0 \tag{29}$$

$$v_0\frac{\partial u_1}{\partial y} + v_1\frac{\partial u_0}{\partial y} = \frac{1}{Re}\left(\frac{\partial^2 u_1}{\partial y^2} + \frac{\partial^2 u_1}{\partial z^2}\right) + Gr\theta_1 + GmC_1 - Mu_1 \tag{30}$$

$$v_0\frac{\partial v_1}{\partial y} = -\frac{\partial p_1}{\partial y} + \frac{1}{Re}\left(\frac{\partial^2 v_1}{\partial y^2} + \frac{\partial^2 v_1}{\partial z^2}\right) \tag{31}$$

$$v_0\frac{\partial w_1}{\partial y} = -\frac{\partial p_1}{\partial z} + \frac{1}{Re}\left(\frac{\partial^2 w_1}{\partial y^2} + \frac{\partial^2 w_1}{\partial z^2}\right) - Mw_1 \tag{32}$$

$$v_0\frac{\partial \theta_1}{\partial y} + v_1\frac{\partial \theta_0}{\partial y} = \frac{1}{RePr}\left(\frac{\partial^2 \theta_1}{\partial y^2} + \frac{\partial^2 \theta_1}{\partial z^2}\right) - F\theta_1 \tag{33}$$

$$v_0\frac{\partial C_1}{\partial y} + v_1\frac{\partial C_0}{\partial y} = \frac{1}{SRe}\left(\frac{\partial^2 C_1}{\partial y^2} + \frac{\partial^2 C_1}{\partial z^2}\right) - K_cC_1 \tag{34}$$

The corresponding boundary conditions become

$$u_1 = 0, v_1 = -\cos(\pi z), w_1 = 0, \theta_1 = 0, C_1 = 0 \text{ at } y = 0$$

$$u_1 = 0, v_1 = 0, w_1 = 0, \theta_1 = 0, C_1 = 0 \text{ at } y = 1 \tag{35}$$

These are the linear partial differential equations describing the three dimensional flow. To solve the equations (30)-(34), we assume velocity components and pressure in the following form

$$u_1(y,z) = u_{11}(y)\cos(\pi z)$$

$$v_1(y,z) = v_{11}(y)\cos(\pi z)$$

$$w_1(y,z) = -\frac{1}{\pi}v_{11}'(y)sin(\pi z) \tag{36}$$

$$p_1(y,z) = p_{11}(y)\cos(\pi z)$$

$$\theta_1(y,z) = \theta_{11}(y)\cos(\pi z)$$

$$C_1(y,z) = C_{11}(y)\cos(\pi z)$$

The functions $v_1$and $w_1$are selected in such a way that the continuity equation (29) is inherently fulfilled. By inserting the expressions given in equation (36) into equations (30)–(34) and equating the coefficients corresponding to similar harmonic components, a system of differential equations is derived as follows

$$v_{11}'' + Rev_{11}' - \pi^2 v_{11} = Rep_{11}' \tag{37}$$

$$v_{11}''' + Rev_{11}'' - (MRe + \pi^2)v_{11}' = Re\pi^2 p_{11} \tag{38}$$

$$\theta_{11}'' + RePr\theta_{11}' - (FRePr + \pi^2)\theta_{11} = RePrv_{11}\theta_0' \tag{39}$$

$$C_{11}'' + SReC_{11}' - (K_cSRe + \pi^2)\,C_{11} = SRev_{11}C_0' \tag{40}$$

$$u_{11}'' + Reu_{11}' - \pi^2 u_{11} = Rev_{11}u_0' - Re(Gr\theta_{11} + GmC_{11}) \tag{41}$$

The corresponding boundary conditions are

$$u_{11} = 0, v_{11} = -1, v'_{11} = 0, \theta_{11} = 0, C_{11} = 0 \text{ at } y = 0$$

$$u_{11} = 0, v_{11} = 0, v'_{11} = 0, \theta_{11} = 0, C_{11} = 0 \text{ at } y = 1 \quad (42)$$

Solutions of the equations (37)-(41) subject to (42) and on using (36) yield.

$$v_1(y,z) = \sum_{i=1}^{4}[B_i e^{-\mu_i y}]\cos(\pi z) \quad (43)$$

$$w_1(y,z) = \frac{1}{\pi}\sum_{i=1}^{4}[B_i \mu_i e^{-\mu_i y}]\sin(\pi z) \quad (44)$$

$$\theta_1(y,z) = \left[E_1 e^{-m_1 y} + E_2 e^{-m_2 y} + \sum_{i=1}^{4} C_i e^{-(\mu_i+\lambda_2)y} - \sum_{i=1}^{4} D_i e^{-(\mu_i+\lambda_1)y}\right]\cos(\pi z) \quad (45)$$

$$C_1(y,z) = \left[E_3 e^{-m_3 y} + E_4 e^{-m_4 y} + \sum_{i=1}^{4} F_i e^{-(\mu_i+\lambda_3)y} - \sum_{i=1}^{4} G_i e^{-(\mu_i+\lambda_4)y}\right]\cos(\pi z) \quad (46)$$

$$u_1(y,z) = \left[E_5 e^{-m_5 y} + E_6 e^{-m_6 y} + \sum_{i=1}^{4} L_i e^{-(\mu_i+\lambda_3)y} - \sum_{i=1}^{4} M_i e^{-(\mu_i+\lambda_4)y} + \sum_{i=1}^{4} N_i e^{-m_i y}{}_1 + \sum_{i=1}^{4} P_i e^{-(\mu_i+\lambda_2)y} + \sum_{i=1}^{4} Q_i e^{-(\mu_i+\lambda_1)y} + \sum_{i=1}^{4} R_i e^{-(\mu_i+\lambda_3)y} + \sum_{i=1}^{4} S_i e^{-(\mu_i+\lambda_4)y}\right]\cos(\pi z), \quad (47)$$

where

$$m_{1,2} = \frac{1}{2}\left\{RePr \pm \sqrt{Re^2Pr^2 + 4(FRePr + \pi^2)}\right\}$$

$$m_{3,4} = \frac{1}{2}\left\{SRe \pm \sqrt{S^2Re^2 + 4(K_cSRe + \pi^2)}\right\}$$

$$m_{5,6} = \frac{1}{2}\left\{SRe \pm \sqrt{S^2Re^2 + 4(MRe + \pi^2)}\right\}$$

$$\mu_{1,2} = \frac{1}{2}\{\lambda_5 \pm \sqrt{\lambda_5^2 + 4\pi^2}\}$$

$$\mu_{3,4} = \frac{1}{2}\{\lambda_6 \pm \sqrt{\lambda_6^2 + 4\pi^2}\}$$

$$r_1 = (\mu_4 - \mu_1)(e^{-\mu_1} - e^{-\mu_3})$$

$$r_2 = (\mu_4 - \mu_2)(e^{-\mu_2} - e^{-\mu_3})$$

$$r_3 = (\mu_3 - \mu_1)(e^{-\mu_1} - e^{-\mu_4})$$

$$r_4 = (\mu_3 - \mu_2)(e^{-\mu_2} - e^{-\mu_4})$$

$$r_5 = \mu_4 e^{-\mu_3},\ r_6 = \mu_3 e^{-\mu_4}$$

$$B_1 = \frac{r_4 r_5 - r_2 r_6}{r_1 r_4 - r_2 r_3},\ B_2 = \frac{r_1 r_6 - r_3 r_5}{r_1 r_4 - r_2 r_3}$$

$$B_3 = \frac{1}{(\mu_3 - \mu_4)}[\mu_4 + (\mu_4 - \mu_1)B_1 + B_2(\mu_4 - \mu_2)]$$

$$B_4 = \frac{-1}{(\mu_3 - \mu_4)}[\mu_3 + (\mu_3 - \mu_1)B_1 + B_2(\mu_3 - \mu_2)] \quad (48)$$

The other constants are not given here to save space.

4. Results and Discussion

Graphs have been prepared to illustrate the variations in velocity, temperature, and concentration distributions for different values of the governing non-dimensional parameters. In the analysis, the Grashof number (Gr) is assumed to be positive, which represents the case of a strongly cooled plate under the influence of buoyancy-driven flow. The Prandtl number is fixed at 0.71, corresponding to air. From a physical standpoint, relatively high values of the Grashof number are considered, as such values are characteristic of natural convection–dominated flows. The Schmidt number (Sc) is chosen to represent different gases, namely helium (Sc = 0.3), water vapor (Sc = 0.60), and ammonia (Sc = 0.78).

The influence of the magnetic parameter, mass Grashof number, thermal Grashof number, chemical reaction parameter, Prandtl number, and Schmidt number on the primary velocity is depicted in Figures 2–7. The results indicate that, for a cooled plate (Gr > 0), the primary velocity diminishes with increasing magnetic parameter, chemical reaction parameter, Prandtl number, and Schmidt number. In contrast, an increase in either the thermal or mass Grashof number enhances the primary velocity. Temperature distributions corresponding to various Reynolds numbers, Prandtl numbers, and radiation parameters are presented in Figures 8–10. The analysis shows that higher values of the Reynolds number, Prandtl number, or radiation parameter lead to a reduction in the temperature field. Figures 11–13 display the concentration profiles for different Schmidt numbers, Reynolds numbers, and chemical reaction parameters. It is observed that the concentration decreases as any of these parameters increase.

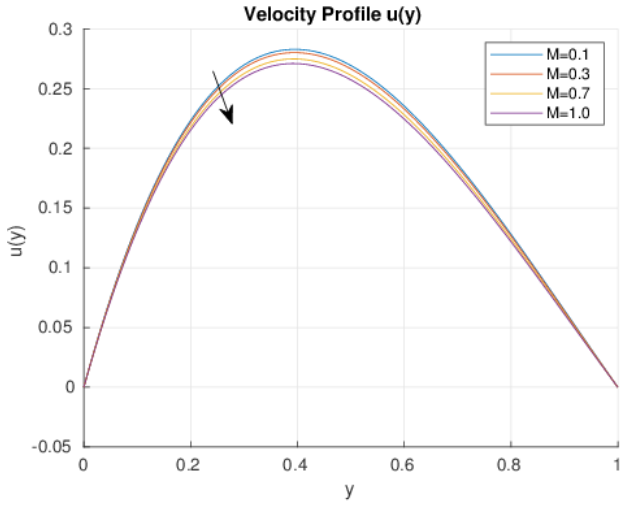

Figure 2. *Primary velocity* u *for* $Gr = 5, Gm = 5, Re = 0.5.$

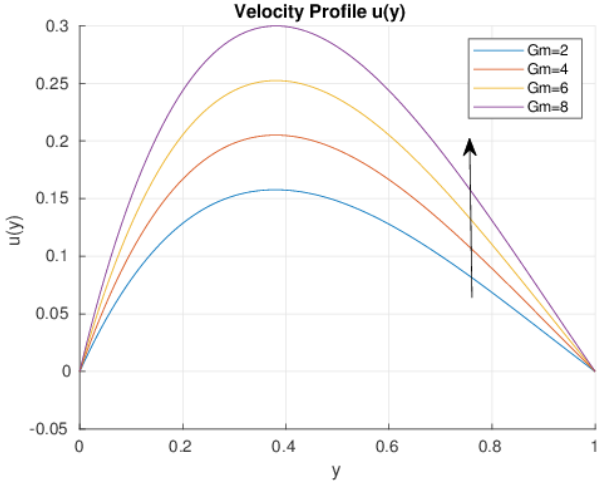

Figure 3. *Primary velocity* u *for* $Gr = 5, M = 5, Pr = 0.71, S = 1, F = 2, Kc = 0.5, \epsilon = 0.05$ $Re = 0.5, Pr = 0.71, S = 1, F = 2, Kc = 0.5, \epsilon = 0.05.$

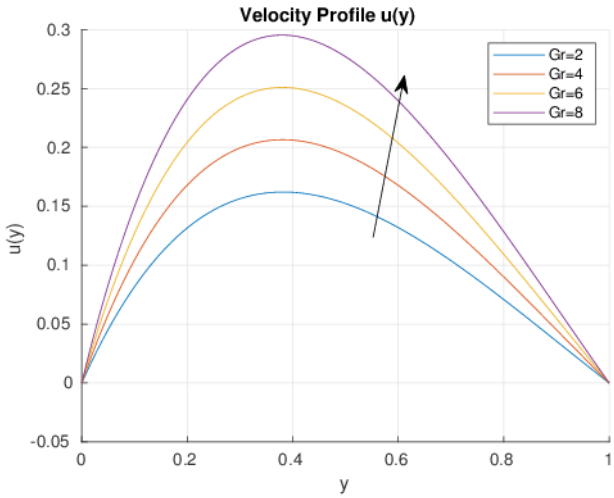

Figure 4. *Primary velocity* u *for* $M = 5, Gm = 5, Re = 0.5.$

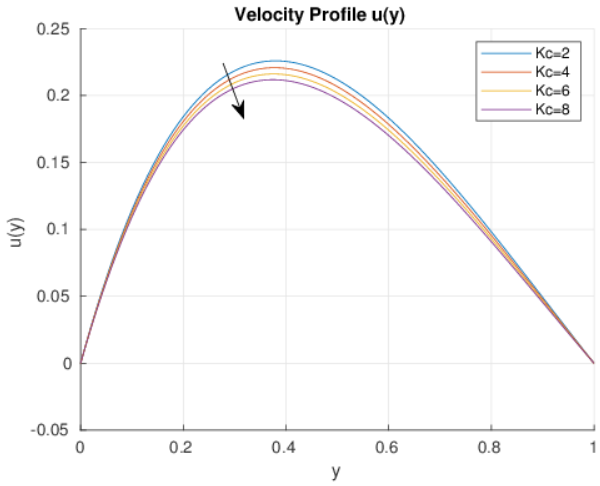

Figure 5. *Primary velocity* u *for* $Gr = 5, Gm = 5, Re = 0.5.$ $Pr = 0.71, S = 1, F = 2, Kc = 0.5, \epsilon = 0.05$ $Pr = 0.71, S = 1, F = 2, M = 5$ $\epsilon = 0.05.$

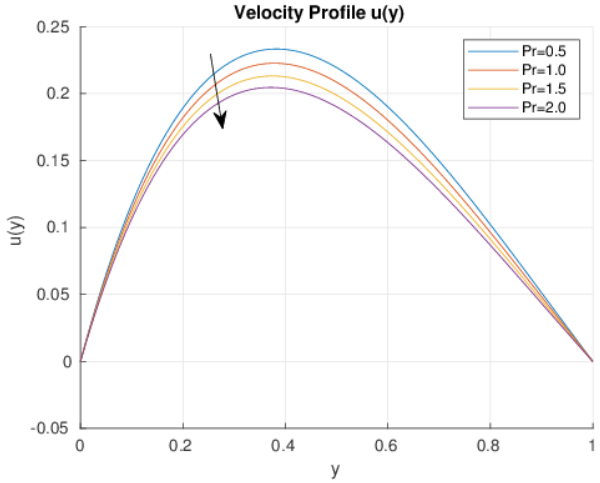

Figure 6. *Primary velocity* u *for* $Gr = 5, Gm = 5.$

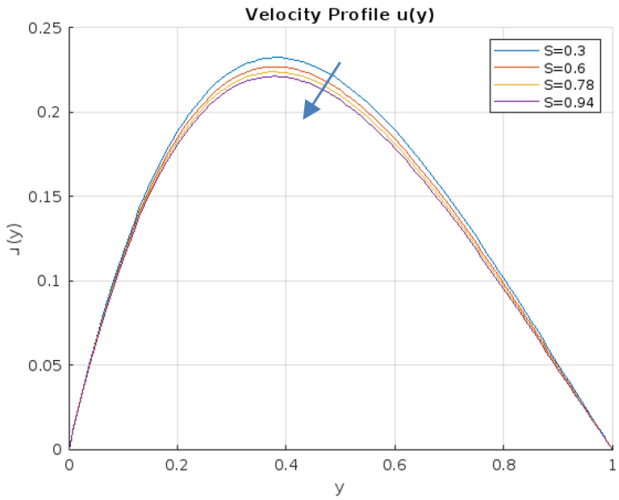

Figure 7. *Primary velocity* u *for* $Gr = 5, Gm = 5, Re = 0.5, M, S = 1, F = 2, Kc = 0.5, \epsilon = 0.05$ $Re = 0.5, Pr = 0.71, M = 1, F = 2, Kc = 0.5, \epsilon = 0.05.$

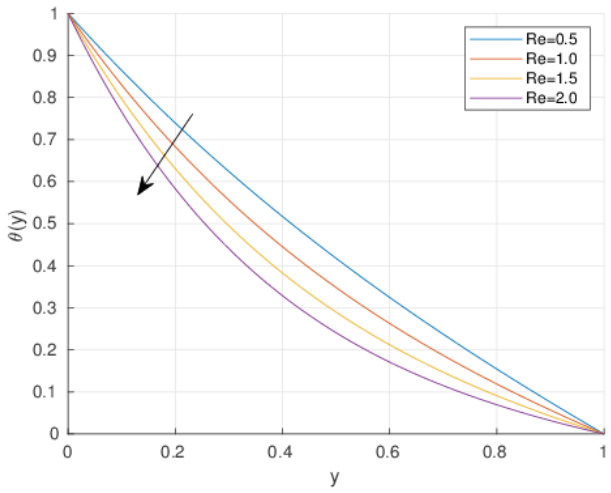

$F = 2, \epsilon = 0.05$

Figure 8. *Temperature profile* θ *for* $Pr = 0.71$.

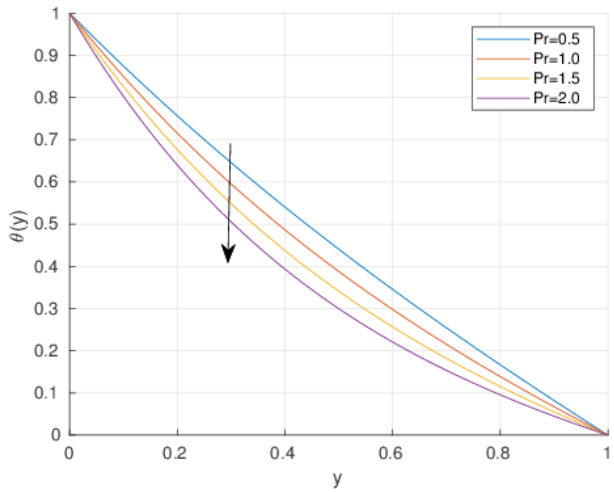

$Pr = 0.71, F = 2, \epsilon = 0.05$

Figure 9. *Temperature profile* θ *for* $Re = 0.5$.

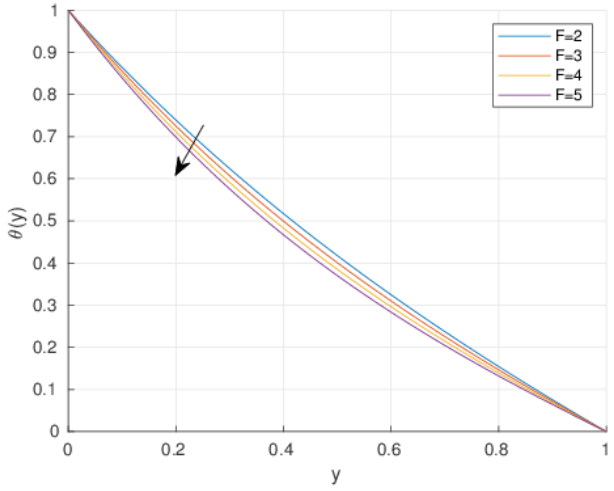

$Pr = 0.71, \epsilon = 0.05$

Figure 10. *Temperature profile* θ *for* $Re = 0.5$.

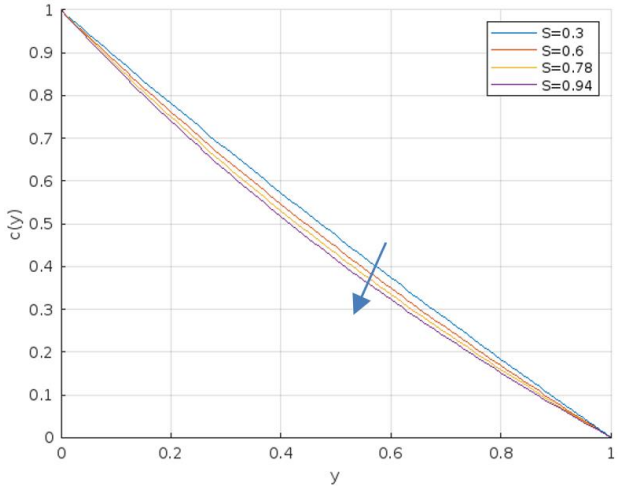

$Kc = 0.5, \epsilon = 0.05$

Figure 11. *Concentration profile* $C(y)$ *for* $Re = 0.5$.

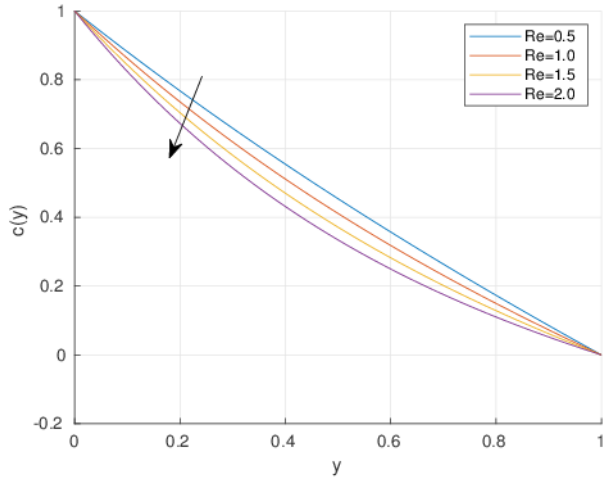

$Kc = 0.5, \epsilon = 0.05$

Figure 12. *Concentration profile* $C(y)$ *for S=1.*

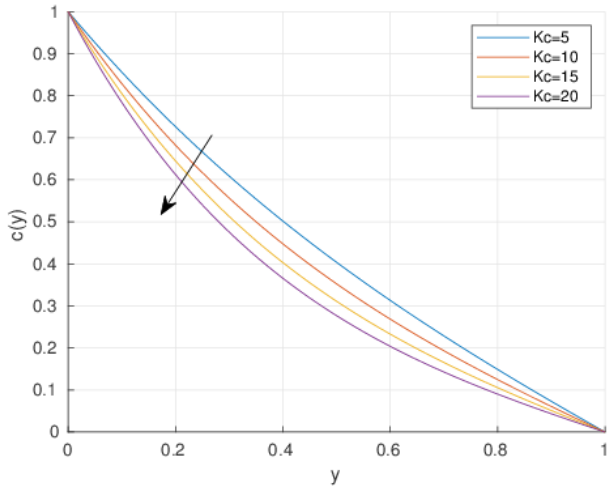

$Kc = 0.5, \epsilon = 0.05$

Figure 13. *Concentration profile* $C(y)$ *for* $Re = 0.5$.

Next, we evaluate the skin friction at the channel boundaries. The shear stress generated by the primary flow at the plate located at $y^* = 0$ is expressed as follows.

$$\tau_x^* = \mu\left(\frac{\partial u^*}{\partial y^*}\right)_{y^*=0} = \frac{\mu V_0}{d}\left(\frac{\partial u}{\partial y}\right)_{y=0} \quad (49)$$

In dimensionless terms, the expression for the shear stress at the boundary $y = 0$ takes the following form.

$$\tau_x = \frac{\tau_x^* d}{\mu V_0} = \left(\frac{\partial u}{\partial y}\right)_{y=0} = u_0'(0) + \epsilon u_1'(0)$$

$$= \sum_{i=1}^{6} -A_i\lambda_i - \epsilon\{E_5 m_5 + E_6 m_6 + \sum_{i=1}^{4} L_i(\mu_i + \lambda_3) + \sum_{i=1}^{4} M_i(\mu_i + \lambda_4) + \sum_{i=1}^{4} N_i m_i + \sum_{i=1}^{4} P_i(\mu_i + \lambda_2) + \sum_{i=1}^{4} Q_i(\mu_i + \lambda_1) + \sum_{i=1}^{4} R_i(\mu_i + \lambda_3) + \sum_{i=1}^{4} S_i(\mu_i + \lambda_4)\}\cos \pi z \quad (50)$$

The shear stress at the plate $y^* = 1$ due to the primary flow is given by

$$\tau_x^* = \mu\left(\frac{\partial u^*}{\partial y^*}\right)_{y^*=1} = \frac{\mu V_0}{d}\left(\frac{\partial u}{\partial y}\right)_{y=1} \quad (51)$$

In non-dimensional form the shear stress at the plate $y = 1$ can be written as

$$\tau_x = \frac{\tau_x^* d}{\mu V_0} = \left(\frac{\partial u}{\partial y}\right)_{y=1} = u_0'(1) + \epsilon u_1'(0), = \sum_{i=1}^{6} -A_i\lambda_i e^{-\lambda_i} - \epsilon\{E_5 m_5 e^{-m_5} + E_6 m_6 e^{-m_6} + \sum_{i=1}^{4} L_i(\mu_i + \lambda_3)e^{-(\mu_i+\lambda_3)} + \sum_{i=1}^{4} M_i(\mu_i + \lambda_4)e^{-(\mu_i+\lambda_4)} + \sum_{i=1}^{4} N_i m_i e^{-m_i} + \sum_{i=1}^{4} P_i(\mu_i + \lambda_2)e^{-P_i(\mu_i+\lambda_2)} + \sum_{i=1}^{4} Q_i(\mu_i + \lambda_1)e^{-(\mu_i+\lambda_1)} + \sum_{i=1}^{4} R_i(\mu_i + \lambda_3)e^{-(\mu_i+\lambda_3)} + \sum_{i=1}^{4} S_i(\mu_i + \lambda_4)\, e^{-(\mu_i+\lambda_4)}\}\cos \pi z \quad (52)$$

The variation of the primary-flow shear stress at the lower plate $y = 0$, represented by τ_{x_0}, is illustrated in Figures 14–19 for different values of the mass Grashof number (Gm), thermal Grashof number (Gr), chemical reaction parameter (Kc), magnetic parameter (M), Reynolds number (Re), and Schmidt number (S), considering the cooling case of the plate (Gr > 0). The results indicate that τ_{x_0} increases as Gr, Gm, Re, or M increase, whereas it decreases with increasing Schmidt number or chemical reaction parameter under cooling conditions.

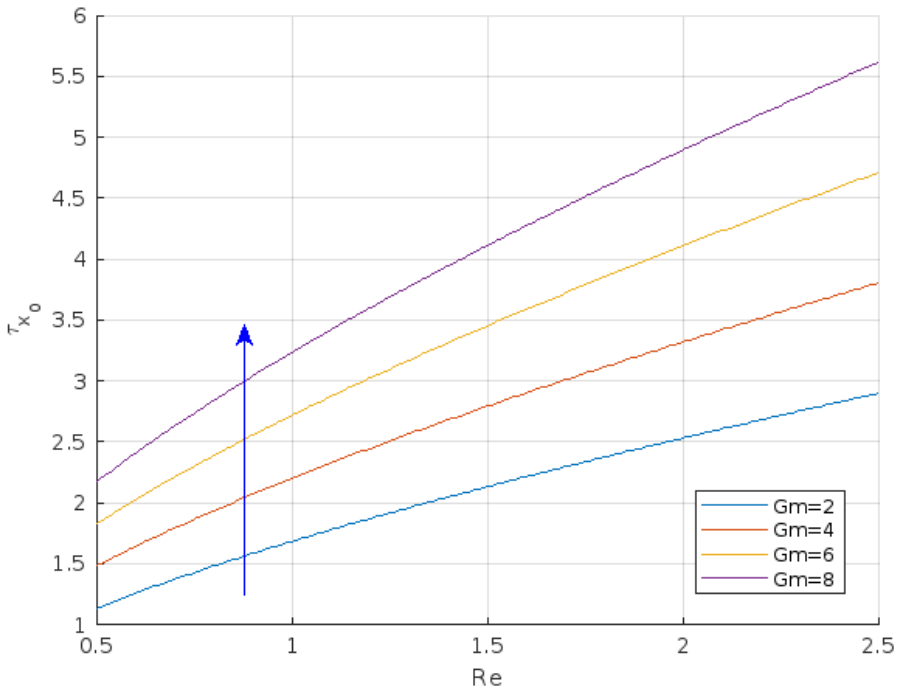

for $Gr = 5, M = 5.0, Kc = 0.5, \epsilon = 0.05$

Figure 14. *Shear stress at* $y = 0$ *due to primary flow.*

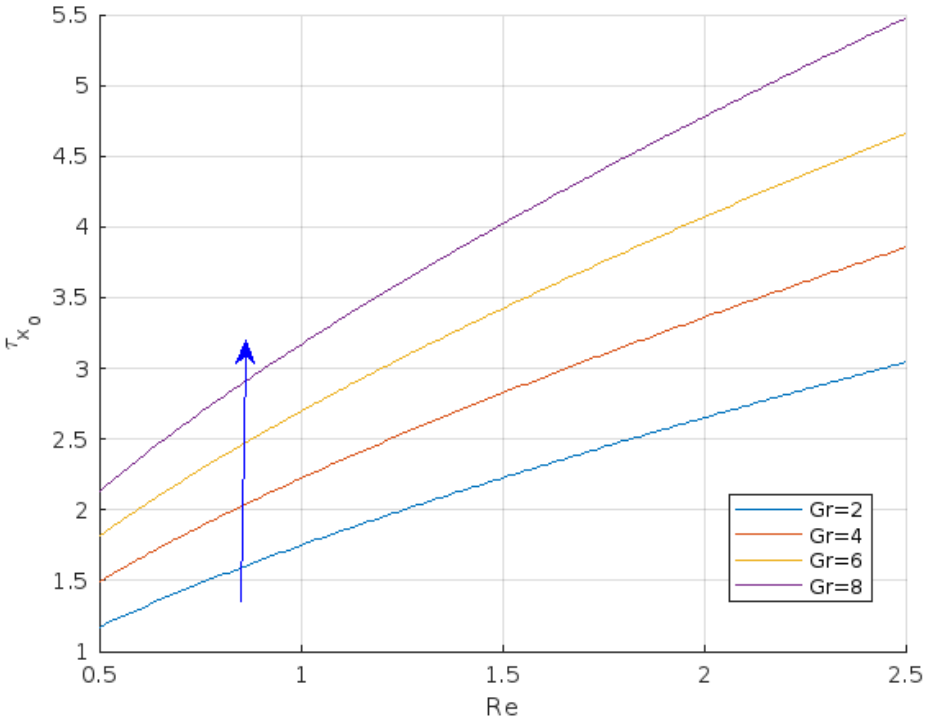

for $Gm = 5, M = 5.0, Kc = 0.5, \epsilon = 0.05$

Figure 15. *Shear stress at* $y = 0$ *due to primary flow.*

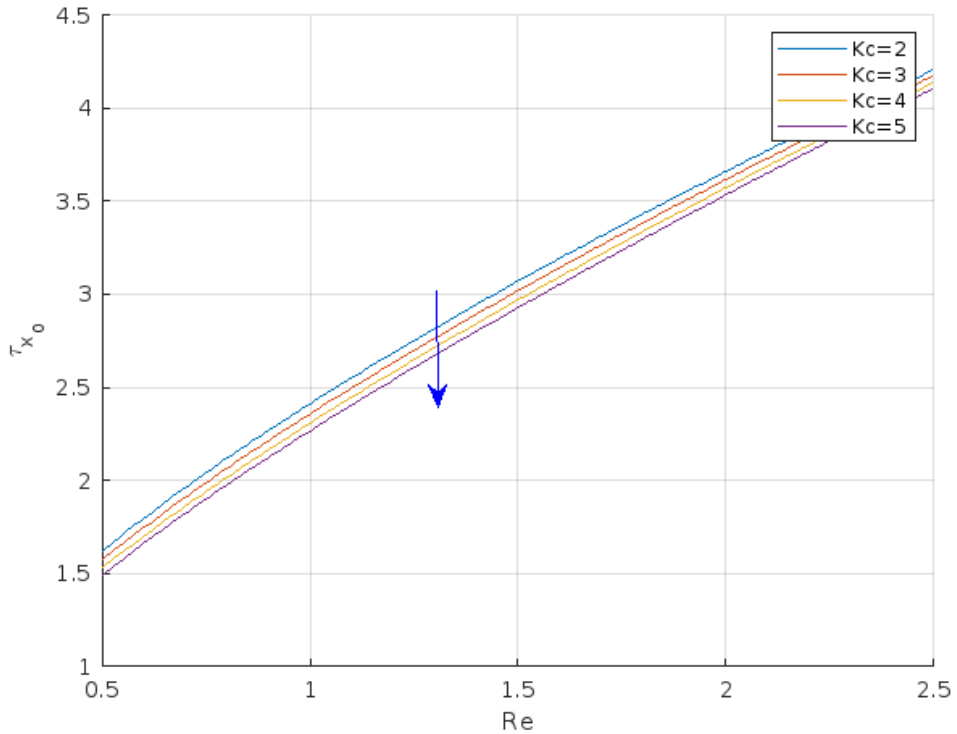

for $Gr = 5, M = 5.0, Gm = 5.0, \epsilon = 0.05$

Figure 16. *Shear stress at* $y = 0$ *due to primary flow.*

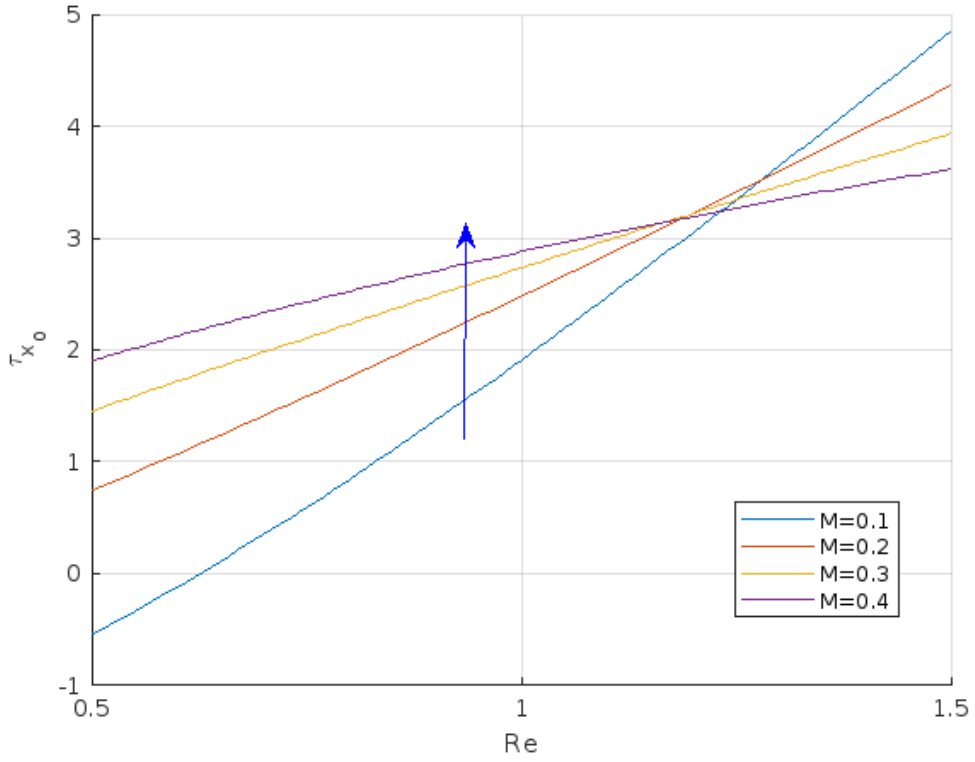

for $Gr = 5, M = 5.0, Gm = 5.0, \epsilon = 0.05$

Figure 17. *Shear stress at* $y = 0$ *due to primary flow.*

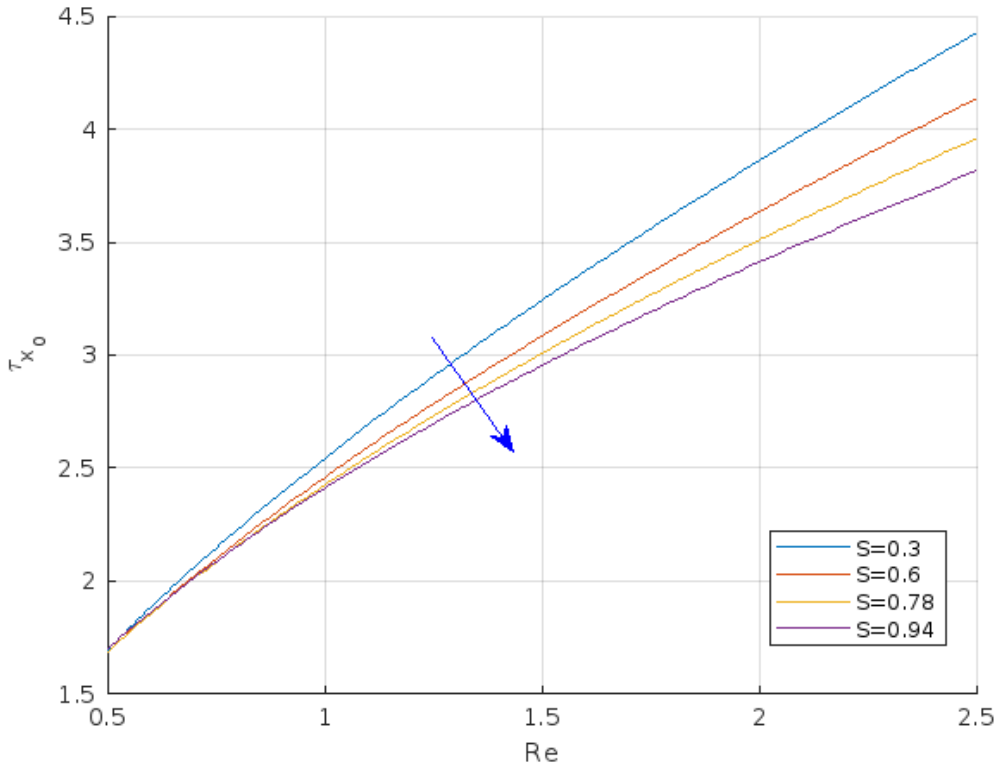

for $Kc = 0.5, Gr = 5, M = 5.0, Gm = 5.0, \epsilon = 0.05$

Figure 18. *Shear stress at* $y = 0$ *due to primary flow.*

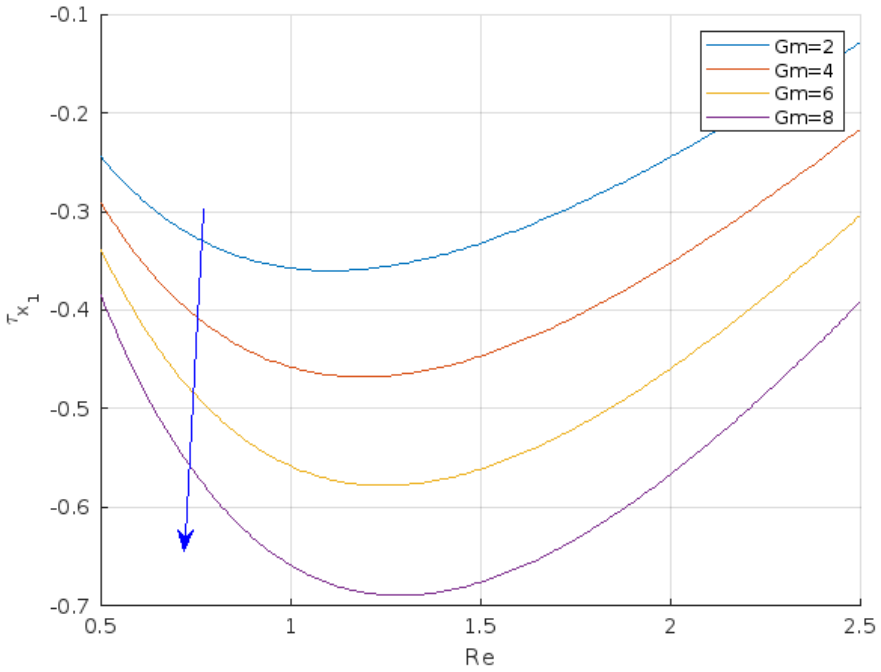

for $Gr = 5, M = 5.0, Kc = 0.5, \epsilon = 0.05$

Figure 19. *Shear stress at* $y = 1$ *due to primary flow.*

Similarly, the shear stress at the upper plate $y = 1$, denoted by τ_{x_1}, is presented in Figures 20–24 for the same range of governing parameters. In this case, τ_{x_1} is found to increase with higher values of the chemical reaction parameter and Schmidt number, while it decreases as the mass Grashof number, thermal Grashof number, or magnetic parameter increase for a cooled plate.

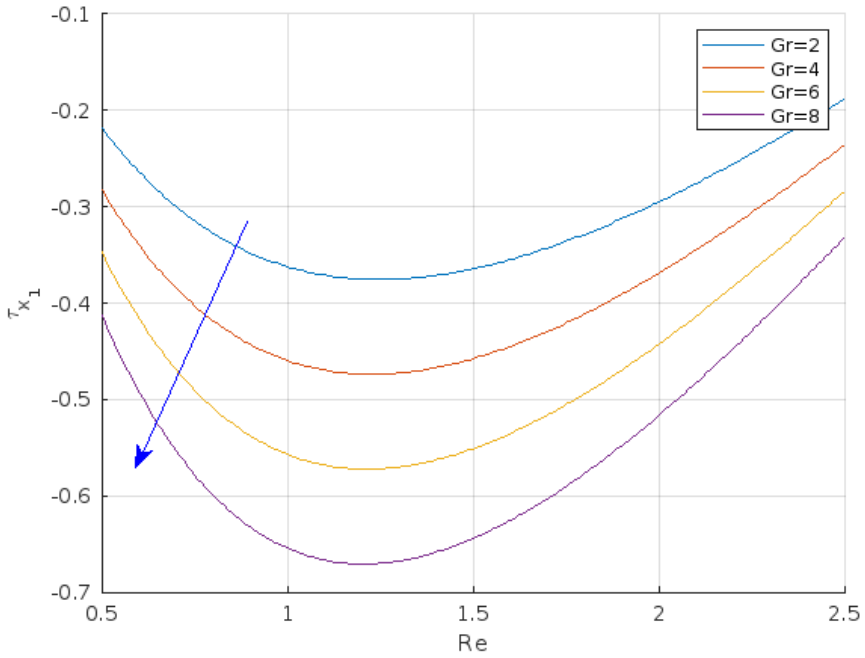

for $Gm = 5, M = 5.0, Kc = 0.5, \epsilon = 0.05$

Figure 20. *Shear stress at* $y = 1$ *due to primary flow.*

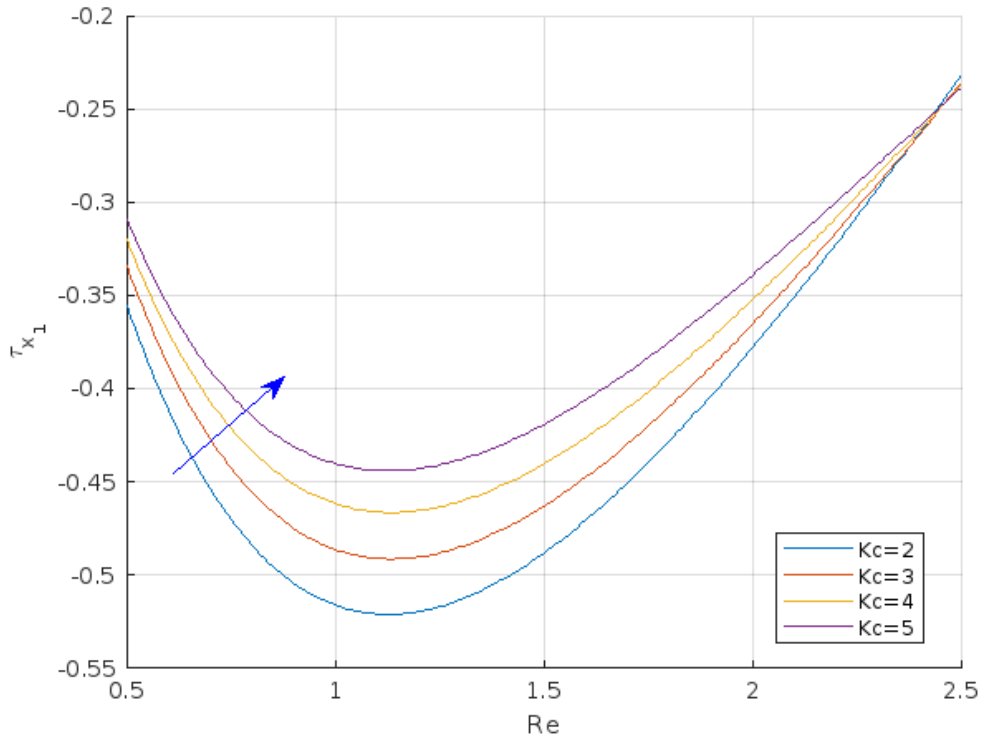

for $Gr = 5, M = 5.0, Gm = 5.0, \epsilon = 0.05$

Figure 21. *Shear stress at* $y = 0$ *due to primary flow.*

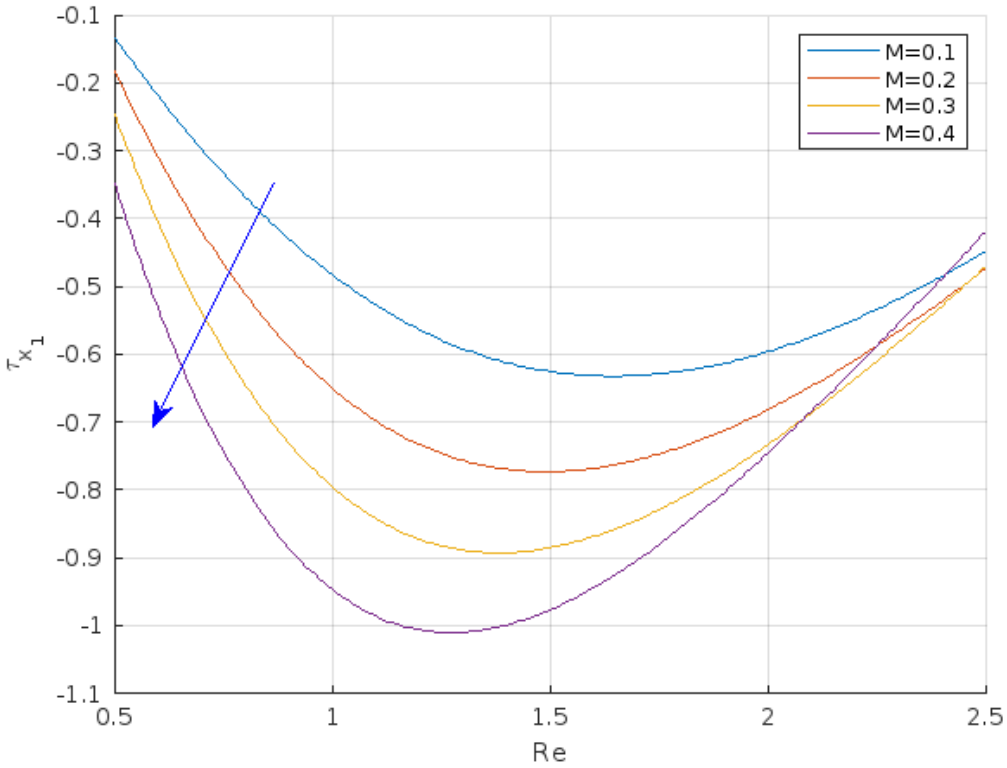

for $Gr = 5, M = 5.0, Gm = 5.0, \epsilon = 0.05$

Figure 22. *Shear stress at* $y = 1$ *due to primary flow.*

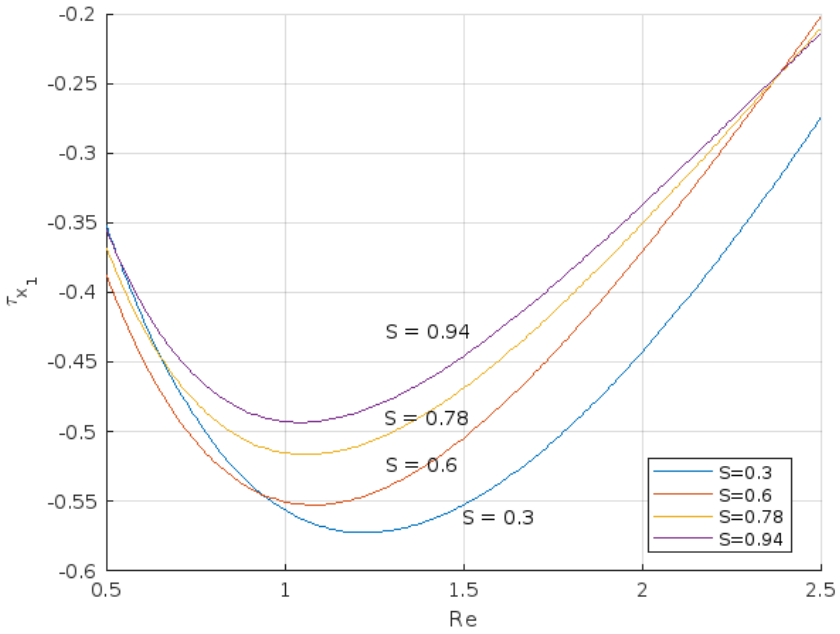

for $Kc = 0.5, Gr = 5, M = 5.0, Gm = 5.0, \epsilon = 0.05$

Figure 23. *Shear stress at* $y = 1$ *due to primary flow.*

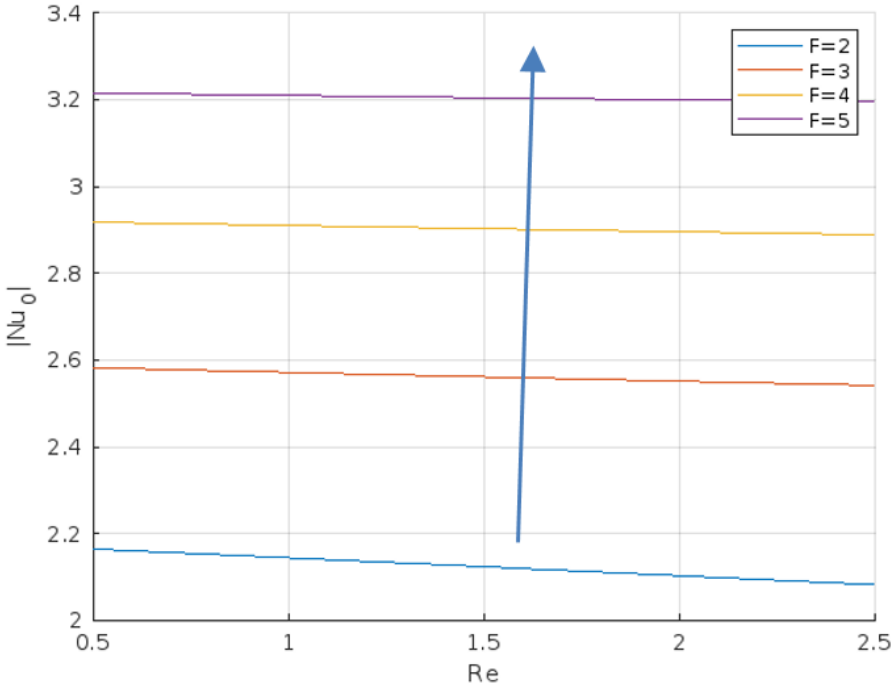

at the plate $y = 0$ for Pr=0.71

Figure 24. *Rate of heat transfer in terms of Nusselt number.*

The Nusselt number serves as an important indicator of the rate of heat transfer between the channel walls and the fluid moving through the space between them. Owing to its engineering significance, it is widely used to quantify convective heat transfer performance. By definition, the Nusselt number is directly related to the heat transfer rate from the plate surface to the adjacent fluid. The convective heat transfer coefficient at the wall, which characterizes the intensity of heat exchange between the plate and the fluid, can be determined as follows.

$$q = -k\left(\frac{\partial T^*}{\partial y^*}\right)_{y^*=0} = -\frac{k(T_w - T_0)}{d}\left(\frac{\partial \theta}{\partial y}\right)_{y=0} \tag{53}$$

Expressed in dimensionless form, the heat transfer coefficient at the plate $y = 0$ can be written as follows.

$$Nu_1 = \frac{qd}{k(T_w - T_0)} = -\left(\frac{\partial\theta}{\partial y}\right)_{y=0} = -\theta_0'(0) - \epsilon\theta_1'(0)$$

$$= \frac{1}{(e^{-\lambda_1} - e^{-\lambda_2})}\left[\lambda_1 e^{-\lambda_2} - \lambda_2 e^{-\lambda_1}\right] - \epsilon[E_1 m_1 + E_2 m_2 + \sum_{i=1}^{4} C_i(\mu_i + \lambda_2) + \sum_{i=1}^{4} D_i(\mu_i + \lambda_1)]cos\pi z \quad (54)$$

and the heat transfer coefficient at the plate $y = 1$ is given by

$$Nu_2 = \frac{qd}{k(T_w - T_0)} = -(\frac{\partial\theta}{\partial y})_{y=1} = -\theta_0'(1) - \epsilon\theta_1'(1)$$

$$= \frac{e^{-(\lambda_1+\lambda_2)}}{(e^{-\lambda_1} - e^{-\lambda_2})}(\lambda_2 - \lambda_1) - \epsilon\left[E_1 m_1 e^{-m_1} + E_2 m_2 e^{-m_2} + \sum_{i=1}^{4} C_i(\mu_i + \lambda_2)e^{-(\mu_i+\lambda_2)} + \sum_{i=1}^{4} D_i(\mu_i + \lambda_1)\, e^{-(\mu_i+\lambda_1)}\right]cos\pi z \quad (55)$$

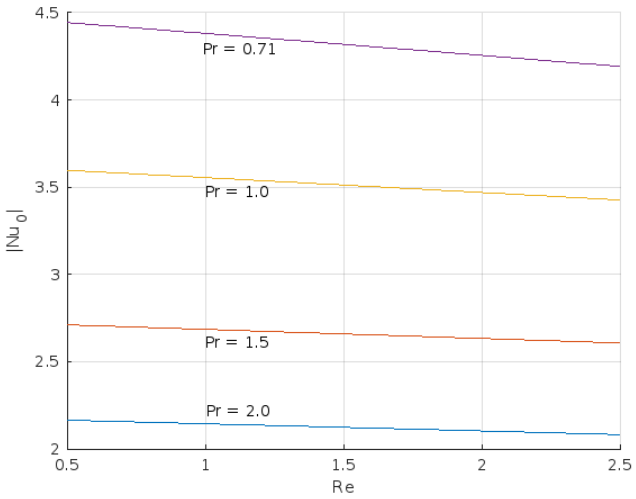

at the plate $y = 0$ for $F = 2$

Figure 25. *Rate of heat transfer in terms of Nusselt number.*

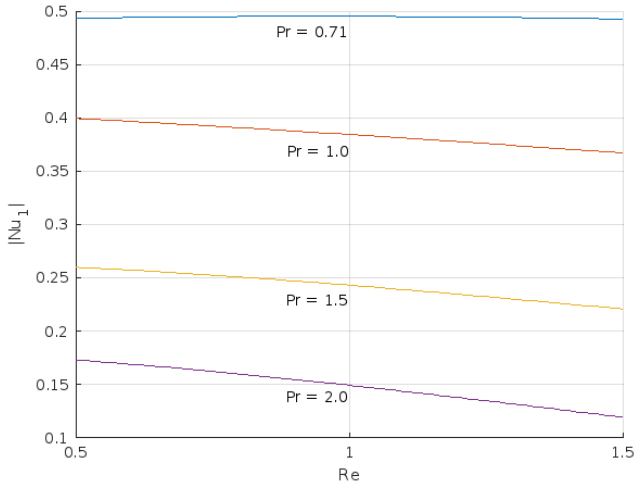

at the plate $y = 1$ for $F = 2$

Figure 26. *Rate of heat transfer in terms of Nusselt number.*

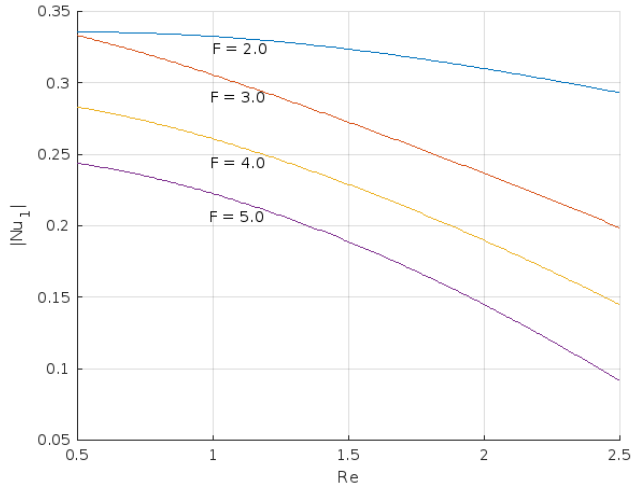

at the plate $y = 1$ for $Pr = 0.71$

Figure 27. *Rate of heat transfer in terms of Nusselt number.*

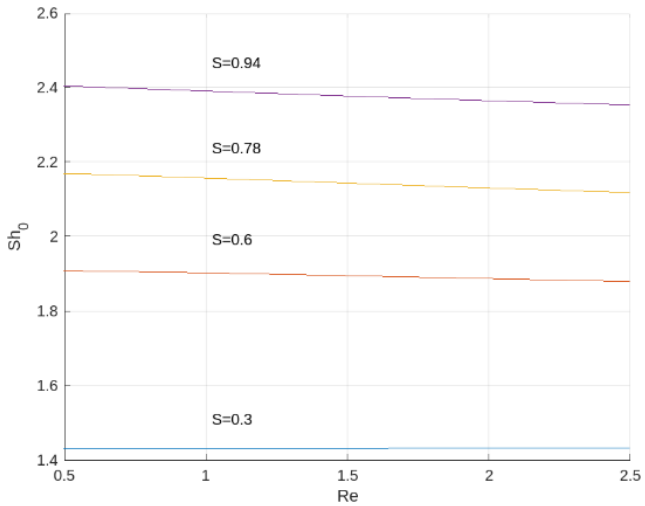

for $Kc = 0.5$

Figure 28. *Sherwood number at the plate* $y = 0$.

The variation of the heat transfer rate, expressed through the Nusselt number, is illustrated for different values of the radiation parameter and Reynolds number, while keeping Gr

= 5.0, $\varepsilon = 0.05$, and $z = 0.0$ fixed (see Figures 24–25). At the lower plate $y = 0$, the Nusselt number increases as the radiation parameter increases, indicating enhanced heat transfer. However, it decreases with an increase in the Prandtl number. For the upper plate $y = 1$, the heat transfer rate, represented by Nu_2, is shown in Figures 25–28. The results reveal that the Nusselt number at this plate decreases with increasing Prandtl number, radiation parameter, and Reynolds number.

In dimensionless form, the mass transfer rate at the plate $y = 0$ can be expressed in terms of the Sherwood number Sh as follows

$$Sh_0 = (\frac{\partial C}{\partial y})_{y=0}$$

$$= -C_0'(0) - \epsilon C_1'(0)$$

$$= -C_0'(0) - \epsilon C_{11}'(0)\cos(\pi z)$$

$$= -\frac{(\lambda_4 e^{-\lambda_3} - \lambda_3 e^{-\lambda_4})}{(e^{-\lambda_4} - e^{-\lambda_3})]} + \epsilon\,[\mathrm{E}_3 m_3 + E_4 m_4 + \sum_{i=1}^{4} F_i(\mu_i + \lambda_3) - \sum_{i=1}^{4} G_i(\mu_i + \lambda_4)] \quad (56)$$

In dimensionless terms, the mass transfer rate at the boundary $y = 1$ is represented by the Sherwood number Sh as given below.

$$Sh_1 = (\frac{\partial C}{\partial y})_{y=1}$$

$$= -C_0'(1) - \epsilon C_1'(1),$$

$$= -C_0'(1) - \epsilon C_{11}'(1)\cos(\pi z),$$

$$= -\frac{(\lambda_4 e^{-\lambda_3} - \lambda_3 e^{-\lambda_4})}{(e^{-\lambda_4} - e^{-\lambda_3})]} + \epsilon[\mathrm{E}_3 m_3 e^{-m_3} + E_4 m_4 e^{-m_4} + \sum_{i=1}^{4} F_i(\mu_i + \lambda_3) e^{-(\mu_i + \lambda_3)} - \sum_{i=1}^{4} G_i(\mu_i + \lambda_4) e^{-(\mu_i + \lambda_4)}] \quad (57)$$

The behavior of mass transfer, represented by the Sherwood number, at both plates $y = 0$ and $y = 1$ is illustrated in Figures 28–31 for various values of the Schmidt number (S), chemical reaction parameter (Kc), and Reynolds number (Re). The results indicate that, at the lower plate $y = 0$, the Sherwood number increases as either the Schmidt number or the chemical reaction parameter increases. In contrast, at the upper plate $y = 1$, the Sherwood number exhibits the opposite trend, decreasing with an increase in these parameters.

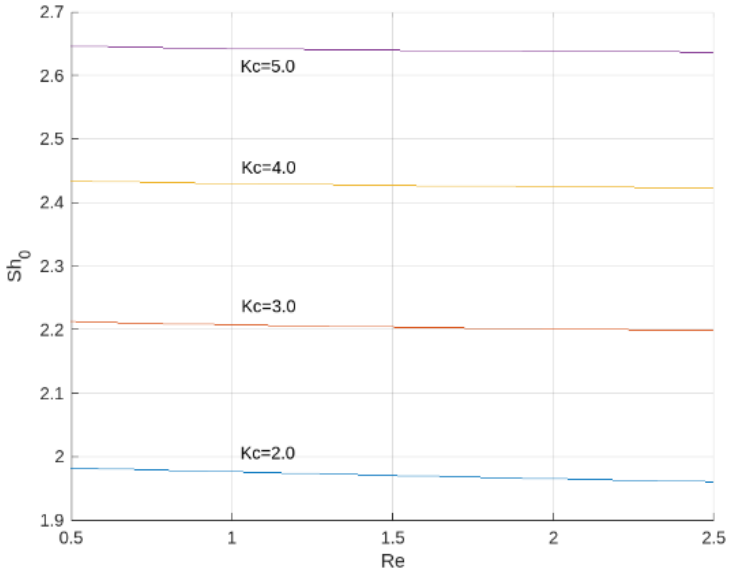

for $S = 0.3$

Figure 29. *Sherwood number at the plate* $y = 0$.

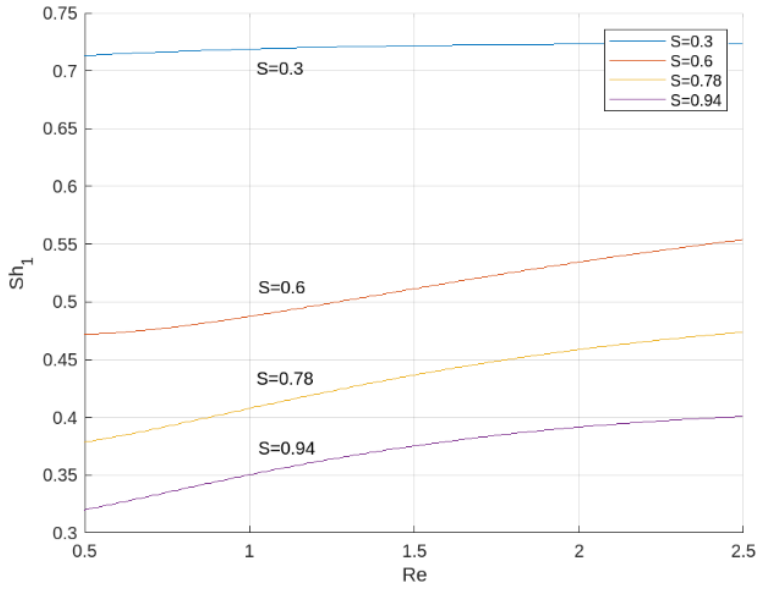

for $Kc = 0.5$

Figure 30. Sherwood number at the plate $y = 1$.

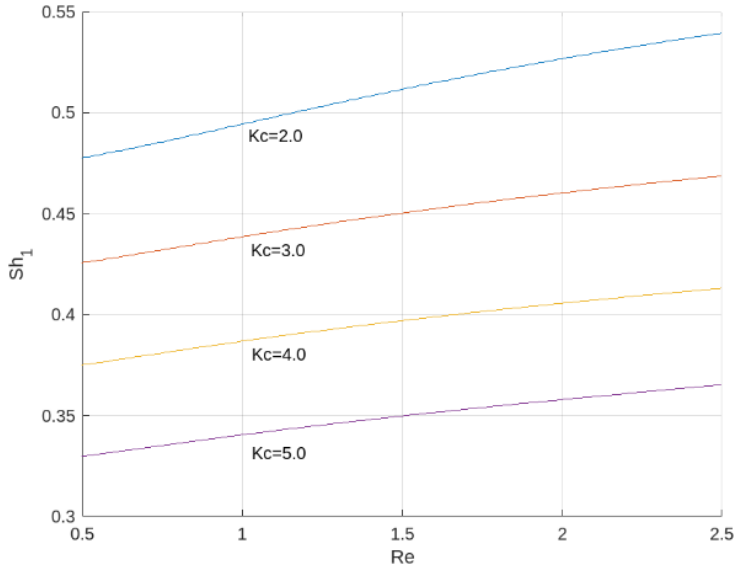

for $S = 0.3$

Figure 31. Sherwood number at the plate $y = 1$.

5. Conclusion

The study investigates heat and mass transfer in a viscous, incompressible fluid flowing through a vertical channel under magnetic field and thermal radiation effects. It is observed that increasing the thermal Grashof number (Gr) enhances fluid velocity due to stronger buoyancy forces caused by temperature differences. Similarly, a higher mass Grashof number increases velocity by intensifying buoyancy effects arising from concentration differences. In contrast, an increase in the chemical reaction parameter reduces both velocity and concentration. This is because chemical reactions alter buoyancy forces and consume solute near the surface, thereby weakening the concentration gradient and overall flow.

Abbreviations

C_p	Specific Heat at Constant Pressure
d,	Channel Width
F,	Radiation Parameter
g,	Gravitational Acceleration
Gr,	Grashoff Number

$K_{1,2}$	Constants
$k,$	Thermal Conductivity
$K^*,$	Chemical Reaction Rate Constants
$m_i, i = 1, \cdots 6$	Constants
$Nu_1, Nu_2,$	Nusselt Number at the Plates $y = 0$ and $y = 1$
p^*	Pressure
$p,$	Dimensionless Pressure
$Pr,$	Prandtl Number
$q,$	Local Heat Transfer at the Plate
$r_i, i = 1, \cdots 4$	Constants
$Re,$	Reynolds Number
$T^*,$	Temperature of the Fluid
$T_w,$	plate Temperature $y^* = 0$
$T_0,$	plate Temperature $y^* = d$
u^*, v^*, w^*	Velocity Components in x^*, y^*, z^* −Axes Respectively
x^*, y^*, z^*	Cartesian Coordinates System
$V_0,$	Constant Suction Velocity
$\mu,$	Viscosity
$\beta,$	Coefficient of Thermal Expansion
$\theta,$	Non-dimensional Temperature
$\nu,$	Kinematic Viscosity
$\varepsilon,$	Amplitude of the Suction Velocity
$\rho,$	Density
τ_x, τ_z	Shear Stress Due to Primary and Secondary Flows

Author Contributions

Sanhita Paul: Data curation, Formal Analysis, Supervision, Writing – review & editing

Mrinmoy Guria: Methodology, Conceptualization, Writing – original draft

Sovan Lal Maji: Formal Analysis, Software, Visualization

Conflicts of Interest

The authors declare no conflicts of interest.

References

[1] Guria, M., Jana, R. N., Three dimensional free convection flow and heat transfer past a vertical channel. International Journal of Fluid Mechanics Research, 33(4) (2006) 320-333. https://doi.org/10.1615/InterJFluidMechRes.v33.i4.20

[2] Takhar H S., Gorla R S R, Soundalgekar V. M., Radiation effects on MHD free convection flow of a radiating gas past a semi-infinite vertical plate. Int J Numer Math Heat Fluid Flow, 6(2), (1996), 77-83. https://doi.org/10.1108/09615539610113118

[3] Guria M, Ghara N and Jana R. N, Radiation effect on three dimensional vertical channel flow. International Journal of Applied Mechanics and Engineering, 15(4), (2010), 1065-1081.

[4] Guria, M, Ghara, N, Jana, R. N., Radiation effect on three dimensional MHD flow past a vertical porous plate. Journal of Physical Sciences. 15, (2011), pp. 161-170.

[5] Singh AK and Thakar HS, Three dimensional heat and mass transfer flow of a viscous fluid with periodic suction velocity. International Journal of Fluid Mechanics Research, 34(3), (2007), 267-286. https://doi.org/10.1615/InterJFluidMechRes.v34.i3.60

[6] Ahmed S, Free and forced convective three-dimensional flow with heat and mass transfer. International Journal of Pure and Applied Mechanics, 5(1), (2008), 26-38.

[7] Ahmed S, Liu, IC, Mixed convective transient three dimensional heat and mass transfer flow with transversely periodic suction velocity. International Journal of Applied Mathematics and Mechanics, 6(1), (2010), 58-73.

[8] Gnaneswara Reddy M and Bhaskar Reddy N, Radiation and mass transfer effects on unsteady MHD free convection flow past a vertical porous plate with viscous dissipation, Int. J. of Appl. Math and Mech., Vol. 6(6), (2010), 96-110.

[9] Guria, M., Heat and mass transfer flow past a vertical porous plate in the presence of radiation. Journal of Physical Sciences, Vol. 20, (2015), 143-158.

[10] Guria, M., Effect of slip condition on vertical channel flow in the presence of radiation. International Journal of Applied Mechanics and Engineering, 21(2), (2016), 341-358. https://doi.org/10.1515/ijame-2016-0021

[11] Guria M.: Heat and mass transfer on three dimensional vertical channel flow in the presence of radiation. Journal of Physical Sciences, vol. 21, pp. 83-97 2017.

[12] Guria, M.: Heat and Mass Transfer on three dimensional flow through vertical channel with slip condition and radiation. IOSR Journal of Mathematics (IOSR-JM). 18(3), (2022), pp. 60-71. https://doi.org/10.9790/5728-1803016071

[13] Guria, M.: Heat and mass transfer in a vertical channel flow through a porous medium in the presence of radiation. Int. J. Applied Mechanics and Engineering. 27(3), (2022), pp. 63-78. https://doi.org/10.2478/ijame-2022-0036

[14] Zigta B. and Koya P. R. (2017): The effect of MHD on free convection with periodic temperature and concentration in the presence of thermal radiation and chemical reaction. − International Journal of Applied Mechanics and Engineering, vol. 22, No. 4, pp. 1059-1073.

[15] Zigta B. (2018): The effect of thermal radiation, chemical reaction and viscous dissipation on MHD flow. International Journal of Applied Mechanics and Engineering, vol. 23, No. 3, pp. 787-801. https://doi.org/10.2478/ijame-2018-0043

[16] Zigta B.: Mixed convection on MHD flow with thermal radiation, chemical reaction and viscous dissipation embedded in a porous medium. International Journal of Applied Mechanics and Engineering, 25(1), 2020, 219-235. https://doi.org/10.2478/ijame-2020-0014

[17] Reddy, G. V. Ramana, Reddy, N. B. and Gorla, R. S. R: Radiation and chemical reaction effect on MHD flow along a moving porous plate. International Journal of Applied Mechanics and Engineering, Vol. 21(1), 2016, pp. 157-168. https://doi.org/10.1515/ijame-2016-0010

[18] Sarma, D. and Mahanta, P. K.: Chemical reaction effects on a three dimensional MHD mass transfer flow past a vertical plate. IOSR Journal of Mathematics, 11(3), 2015, 01-13. https://doi.org/10.9790/5728-11340113

[19] N. Niranjana, N., Vidhya, M., Govindarajan, A. and Rashid, A. M.: Effect of mass transfer and chemical reaction on three dimensional flow through porous medium with heat transfer and heat source. AIP Conference Proceedings, 2277, 030013 (2020). https://doi.org/10.1063/5.0025758